

# Accurate numerical resolution of transients in initial-boundary value problems for the heat equation

Natasha Flyer <sup>\*,1</sup>, Bengt Fornberg <sup>2</sup>

*Department of Applied Mathematics, University of Colorado, 526 UCB, Boulder, CO 80309, USA*

Received 19 March 2002; received in revised form 18 September 2002; accepted 12 October 2002

---

## Abstract

If the initial and boundary data for a PDE do not obey an infinite set of compatibility conditions, singularities will arise in the solution at the corners of the initial time–space domain. For dissipative equations, such as the 1-D heat equation or 1-D convection–diffusion equations, the impacts of these singularities are short lived. However, they can cause a very severe loss of numerical accuracy if we are interested in transient solutions. The phenomenon has been described earlier from a theoretical standpoint. Here, we illustrate it graphically and present a simple remedy which, with only little extra cost and effort, restores full numerical accuracy.

© 2002 Elsevier Science B.V. All rights reserved.

*Keywords:* PDE; Initial-boundary value problem; Corner singularity; Heat equation; Chebyshev method

---

## 1. Introduction

Solutions to initial-boundary value problems (IBVPs) will feature ‘corner singularities’ unless an infinite number of compatibility conditions, connecting the initial- and boundary data, are satisfied. Since the two data sets usually arise from different considerations, each presents independent conditions at the corners of the time–space domain. Therefore, these singularities are almost always present [3]. Although the mathematical literature on the regularity of solutions for IBVPs goes back to the 1930s (for an extensive survey, see [1]), effective numerical remedies have not yet been presented. Reasons include:

- For dissipative equations, the errors that are caused by these initial time–space corner singularities are short-lived.
- When using finite difference or finite element schemes, the truncation errors are usually so large that they dominate this additional error source.

---

\* Corresponding author.

*E-mail addresses:* [flyer@colorado.edu](mailto:flyer@colorado.edu) (N. Flyer), [fornberg@colorado.edu](mailto:fornberg@colorado.edu) (B. Fornberg).

<sup>1</sup> The work was supported by a Post-Doctoral Fellowship under the NSF Grant DMS-9810751 (VIGRE).

<sup>2</sup> The work was additionally supported by the NSF Grant DMS-0073048, and by a Faculty Fellowship from University of Colorado at Boulder.

However nowadays, with spectral and high order methods readily available to provide high accuracy for smooth solutions, these corner singularities can easily come to dominate other sources of errors by 10 orders of magnitude or more. Furthermore, with today’s technology, computing very brief transients accurately has become important in applications such as biophysics [5], nuclear reactor systems [6], computer science-microchip design [2], and transport through porous media [7]. It is therefore necessary not only to understand well the nature of these singularities, but also to have an easy-to-apply remedy which restores high numerical accuracy. We focus in this study on the 1-D heat equation, in order to most easily illustrate both the phenomenon and a correction procedure for it. In Section 2, we derive the analytic expressions for the corner singularities, and illustrate them graphically. In Section 3, we introduce two test examples, and then apply the Chebyshev pseudospectral method (CPS) to numerically solve them. In the first example the BCs and initial condition (IC)/PDE are compatible to all orders, and thus the problem is entirely free of corner singularities. In the second example, singularities of different severities are present in the two corners. When we apply the CPS method, the errors caused by these singularities dominate very strongly over all other error sources. After the correction procedure described in Section 4 has been applied, accuracy with near machine precision is restored also during the initial moments of the simulation. It should be noted that these initial transients are the ones that feature the sharpest gradients of the solution in both time and space. In some applications, they therefore become the most critical moments. The correction method we have described can be generalized in different ways. Section 5 shows how the procedure can be adjusted to apply to variable coefficient 1-D convection–diffusion equations and an example is given that models diffusion through a media that has a sharp gradient in its permeability. The final Section 6 offers some concluding remarks.

## 2. Nature of a corner singularity

Until we consider generalizations in Section 5, we use as our model problem the regular 1-D heat equation on  $[0, 1] \times [0, 1]$

$$u_t = u_{xx} \tag{1}$$

with Dirchlet BCs. We first consider one corner, for example  $(0, 0)$ . At this corner

$$\frac{\partial^k u_{BC}}{\partial t^k} - \frac{\partial^{2k} u_{IC}}{\partial x^{2k}} = \beta_k, \quad k = 0, 1, 2, \dots, \tag{2}$$

where the PDE imposes that  $\beta_k = 0$  for all  $k$ , otherwise there is an incompatibility between the BC and the IC. The key ingredient in our corner correction procedure is to find a simple function,  $s(x, t)$ , which satisfies the PDE away from the corner but has the same incompatibilities as (2) at the corner. The solution will then be represented as  $u(x, t) = s(x, t) + v(x, t)$ , where  $v(x, t)$  satisfies the PDE, has the same IC as  $u(x, t)$  but BCs that are compatible to all orders. Numerical computation is then performed on  $v(x, t)$  which is free of corner singularities. Our starting point to construct  $s(x, t)$  is to find basis functions  $u_k(x, t)$  with the properties

(i)  $u_k(x, t)$  satisfies the PDE away from the corner, (3)

(ii)  $u_k(x, 0) \equiv 0$ ,

(iii)  $\frac{1}{k!} \frac{\partial^j u_k(0, t)}{\partial t^j} = \begin{cases} 1 & \text{for } j = k, \\ 0 & \text{for } j \neq k. \end{cases}$

We then define  $s(x, t)$  as a linear combination of the basis functions  $u_k(x, t)$ :

$$s(x, t) = \sum_{k=0}^{\infty} \frac{\beta_k}{k!} u_k(x, t).$$

reproducing the corner singularity exactly. For Neumann BCs, only condition (iii) in (3) changes so that the basis functions satisfy

$$(iii) \quad \frac{1}{k!} \left( \frac{\partial^j}{\partial t^j} \left\{ \frac{\partial u_k(0, t)}{\partial x} \right\} \right) = \begin{cases} 1 & \text{for } j = k, \\ 0 & \text{for } j \neq k. \end{cases}$$

Then,

$$v(x, t) = \sum_{k=0}^{\infty} \frac{\alpha_k}{k!} u_k(x, t),$$

where

$$\frac{\partial^k}{\partial t^k} \left\{ \frac{\partial u_{BC}}{\partial x} \right\} - \frac{\partial^{2k+1} u_{IC}}{\partial x^{2k+1}} = \alpha_k, \quad k = 0, 1, 2, \dots$$

For the remainder of the paper, only Dirichlet BCs will be considered. In the case of (1),  $u_k(x, t)$  can be found explicitly as follows. To begin, notice that (1) is a linear constant coefficient equation. Therefore, if it is satisfied by a function  $u(x, t)$ , it will also be satisfied by a number of other functions that we can generate from it, such as  $u_x, u_{xx}, \dots, u_t, u_{tt}, \dots, \int_x^x u dx, \int_x^x u dx, \int_t^t u dt, \int_t^t u dt, \dots$ . From the well-known solution to (1) with a delta function IC,  $u(x, t) = \frac{1}{\sqrt{\pi t}} e^{-x^2/(4t)}$ , it then follows that

$$u_0(x, t) = \int_x^{\infty} u(x, t) dx = \operatorname{Erfc}\left(\frac{x}{2\sqrt{t}}\right) \quad (4)$$

also satisfies (1). Considering the first quadrant in the  $(x, t)$ -plane, this solution  $u_0(x, t)$  satisfies the IC  $u_0(x, 0) = 0$  ( $x > 0$ ) and the BC  $u_0(0, t) = 1$  ( $t > 0$ ). To represent higher-order corner singularities (i.e., higher-order basis functions  $u_k(x, t)$ ), (4) is repeatedly integrated from zero to  $t$ . The result is a sequence of functions  $u_k(x, t) = k \int_0^t u_{k-1}(x, t) dt$  which all obey the same IC, i.e.,  $u_k(x, 0) = 0$  ( $x > 0$ ), but the different BC  $u_k(0, t) = t^k$  or in other words  $\frac{1}{k!} (\partial^k u_k(0, t) / \partial t^k) = 1$  ( $t > 0$ ). The functions  $u_k(x, t)$  are readily available in closed form:

$$\begin{aligned} u_0(x, t) &= \operatorname{Erfc}\left(\frac{x}{2\sqrt{t}}\right), \\ u_1(x, t) &= -\sqrt{\frac{t}{\pi}} x e^{-x^2/(4t)} + \left(t + \frac{x^2}{2}\right) \operatorname{Erfc}\left(\frac{x}{2\sqrt{t}}\right), \\ u_2(x, t) &= -\frac{1}{6} \sqrt{\frac{t}{\pi}} x (10t + x^2) e^{-x^2/(4t)} + \left(t^2 + tx^2 + \frac{x^4}{12}\right) \operatorname{Erfc}\left(\frac{x}{2\sqrt{t}}\right), \\ u_3(x, t) &= -\frac{1}{60} \sqrt{\frac{t}{\pi}} x (132t^2 + 28tx^2 + x^4) e^{-x^2/(4t)} + \left(t^3 + \frac{3}{2}t^2x^2 + \frac{1}{4}tx^4 + \frac{x^6}{120}\right) \operatorname{Erfc}\left(\frac{x}{2\sqrt{t}}\right), \\ u_4(x, t) &= -\frac{1}{840} \sqrt{\frac{t}{\pi}} x (2232t^3 + 740t^2x^2 + 54tx^4 + x^6) e^{-x^2/(4t)} \\ &\quad + \left(t^4 + 2t^3x^2 + \frac{1}{2}t^2x^4 + \frac{1}{30}tx^6 + \frac{x^8}{1680}\right) \operatorname{Erfc}\left(\frac{x}{2\sqrt{t}}\right), \text{ etc.}, \end{aligned} \quad (5)$$

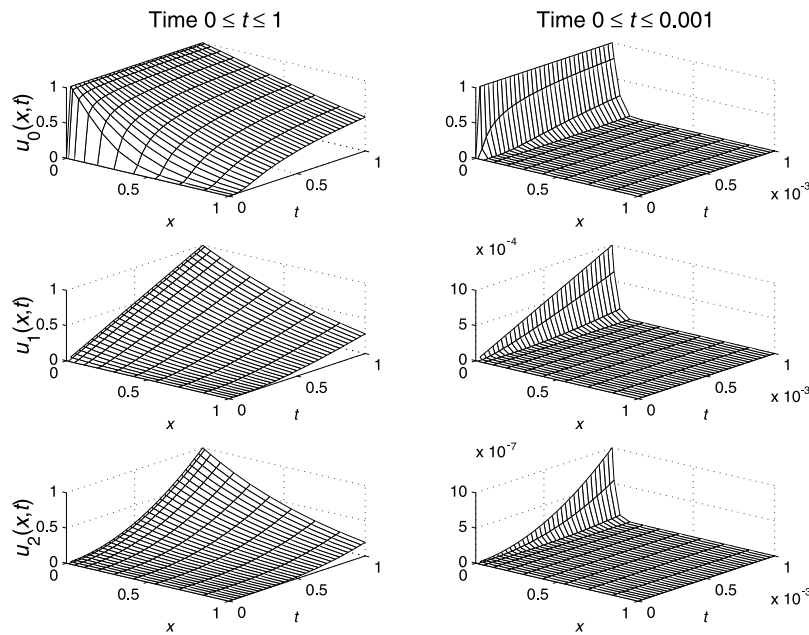


Fig. 1. The functions  $u_0(x, t)$ ,  $u_1(x, t)$ ,  $u_2(x, t)$  displayed over  $0 \leq x \leq 1$ . The time interval for the left subplots is  $0 < t \leq 1$  and for the right ones  $0 \leq t \leq 0.001$ . Note the different vertical scales on the latter.

The left column of subplots in Fig. 1 displays the three first of these functions (i.e.,  $u_0(x, t)$ ,  $u_1(x, t)$ , and  $u_2(x, t)$ ) over the unit square  $[0, 1] \times [0, 1]$  in the  $(x, t)$ -plane. The function  $u_0(x, t)$  shows a very strong singularity at the origin. The data are discontinuous there, but the solution still needs to be infinitely differentiable even at the smallest distance away from this point. The next two functions  $u_1(x, t)$  and  $u_2(x, t)$  superficially look smooth, but this impression is due only to the graphical scale, as the right column of subplots in Fig. 1 reveals. Notice that  $u_1(x, t)$  grows linearly as a function of  $t$  at  $x = 0$ ,  $u_2(x, t)$  grows quadratically and so forth, as is needed to satisfy (iii) in (3). The first three functions  $u_k(x, t)$ ,  $k = 0, 1, 2$ , violate  $u_{BC} - u_{IC} = 0$ ,  $(u_t)_{BC} - (u_{xx})_{IC} = 0$ , and  $(u_{tt})_{BC} - (u_{xxxx})_{IC} = 0$ , respectively. Whenever any condition of this type is violated, there will arise a corner singularity. The only issue is whether the scale on which it appears is such it can be ignored or not. That depends on the application and its accuracy requirements. If we need to take the singularity into account, we need an efficient numerical procedure for doing so. That issue will be discussed in Section 4. Before that, we pose two test problems.

### 3. Two test examples

In both of the examples below, we want to solve (1) over  $0 \leq x \leq 1$  together with the following time periodic Dirichlet boundary conditions:

$$\begin{aligned}
 u(0, t) &= \cos \frac{\pi^2}{2} t, \\
 u(1, t) &= \sin \frac{\pi^2}{2} t.
 \end{aligned}
 \tag{6}$$

It can easily be verified that the combination (1) and (6) is satisfied by

$$u(x, t) = \frac{(1 + e^{\pi/2}) e^{-\pi/2(x-1)} \cos\left(\frac{\pi}{2}(\pi t - x)\right) + (1 - e^{\pi/2}) e^{(\pi/2)x} \cos\left(\frac{\pi}{2}(\pi t + x)\right)}{1 + e^{\pi}}. \quad (7)$$

**Example 1.** Free of corner singularities

Setting  $t = 0$  in (7) gives

$$u(x, 0) = \frac{(1 + e^{\pi/2}) e^{-\pi/2(x-1)} + (1 - e^{\pi/2}) e^{(\pi/2)x}}{1 + e^{\pi}} \cos\frac{\pi}{2}x \quad (0 < x \leq 1). \quad (8)$$

If we take this as the IC, the closed-form solution (7) assures compatibility between the PDE, IC and BC, and makes this example entirely free from corner singularities. The analytic solution up to time  $t = \frac{4}{\pi}$  (one time period) is shown in Fig. 2.

**Example 2.** Presence of corner singularities.

Here, the same BCs are used but this time with the simple IC

$$u(x, 0) = x(x - 1) \quad (0 < x \leq 1). \quad (9)$$

*Analytic solution.* As we will shortly determine, this example features singularities of different severity at the two corners. Again, the solution is known in closed form:

$$u(x, t) = \text{long term solution } (u_L(x, t)) + \text{transient solution } (u_T(x, t)),$$

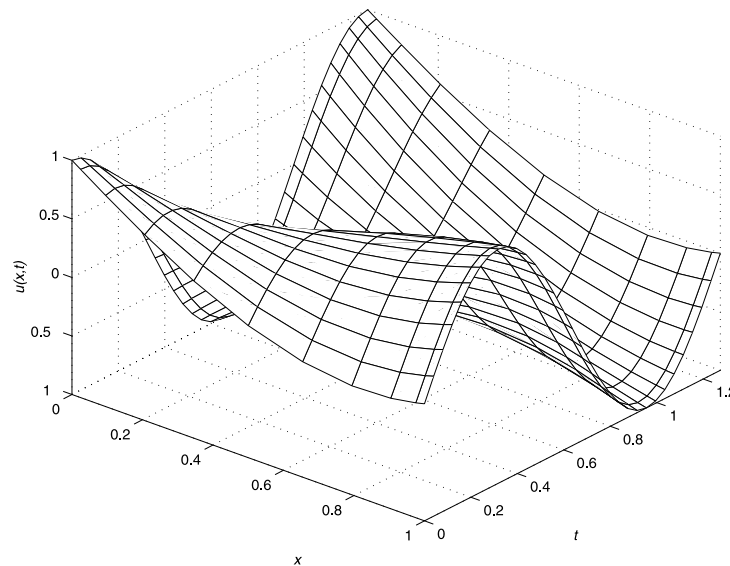


Fig. 2. Analytic solution to Example 1 over one period in time ( $0 \leq t \leq 4/\pi$ ).

where

$$\begin{aligned}
 u_L(x, t) &= \frac{(1 + e^{\pi/2}) e^{-\pi/2(x-1)} \cos\left(\frac{\pi}{2}(\pi t - x)\right) + (1 - e^{\pi/2}) e^{\pi/2x} \cos\left(\frac{\pi}{2}(\pi t + x)\right)}{1 + e^\pi}, \\
 u_T(x, t) &= -\frac{4}{\pi} \sum_{k=1}^{\infty} \frac{k(1 + 2k^2)}{1 + 4k^4} e^{-k^2\pi^2 t} \sin(k\pi x) - \frac{8}{\pi^3} \sum_{k=1, \text{odd}}^{\infty} \frac{e^{-k^2\pi^2 t}}{k^3} \sin(k\pi x).
 \end{aligned}
 \tag{10}$$

The first part or long-term solution is exactly the same as (7). The two infinite Fourier sums, which compose the transient solution, compensate for the different choice of IC that this time is incompatible with the given BCs. The first Fourier sum converges only as  $1/k$  at  $t = 0$ , reflecting that there is a discontinuity between the IC and BC, i.e.,  $u_{BC} \neq u_{IC}$ . Fig. 3 shows the analytic solution of this problem up to time  $t = \frac{4}{\pi}$ , and Fig. 4 its second derivative  $u_{xx}$  up to four different time levels. The discontinuity in  $u(x, t)$  at the origin  $x = 0, t = 0$  causes sharp gradients around that corner. The next order singularity, visible only in the  $u_{xx}$  plots, also produces irregularities which for small  $t$  will greatly decrease the accuracy of any spectral or high-order method.

*Numerical solution.* It is entirely straightforward to implement CPS for the two test examples (see for example [4] for implementation considerations). Therefore, we do not elaborate on any such details here. For time integration, we have used the standard fourth-order Runge–Kutta scheme with sufficiently small time step, so that all visible errors come from the space discretization. Fig. 5 shows the errors for the two test examples when using CPS with  $N = 11$  points in space. In Example 1, the error stays below  $5 \times 10^{-11}$  and the plot over a short time interval does not show any kind of initial anomaly. In the sharpest contrast to this, the display for Example 2 (bottom left subplot) shows a corner anomaly that is 9 orders of magnitude larger than errors in the solution at later times given by Example 1. The lower right subplot shows the ‘final remains’ of the anomaly at time  $t = 0.03$  having decayed to  $O(10^{-6})$ , with the error polluting the entire  $x$  axis. Before proceeding to the next section where we describe a very effective correction procedure for obtaining full accuracy even in the presence of corner singularities, let us remark that mesh refinement in space for the usually very effective CPS method is an inefficient approach. Not only is it very expensive computationally (because implicit time stepping requires the solution of full linear systems, and explicit time stepping suffers

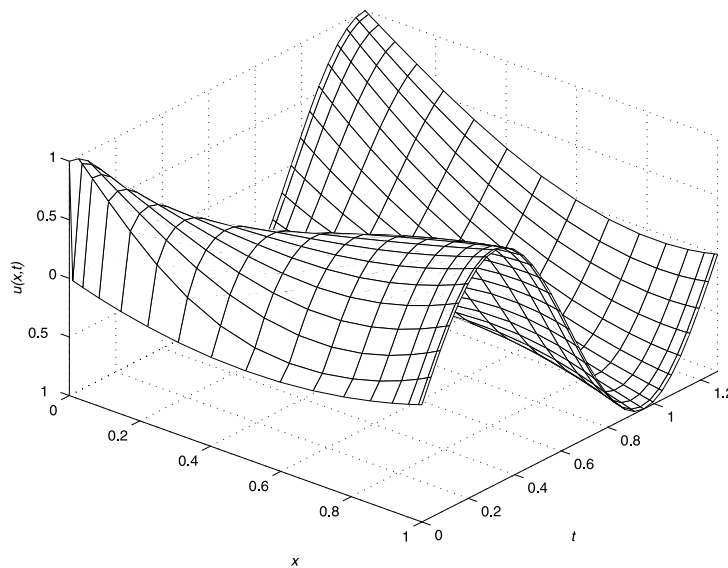


Fig. 3. Analytical solution to Example 2 over the interval  $0 \leq t \leq \pi/4$ .

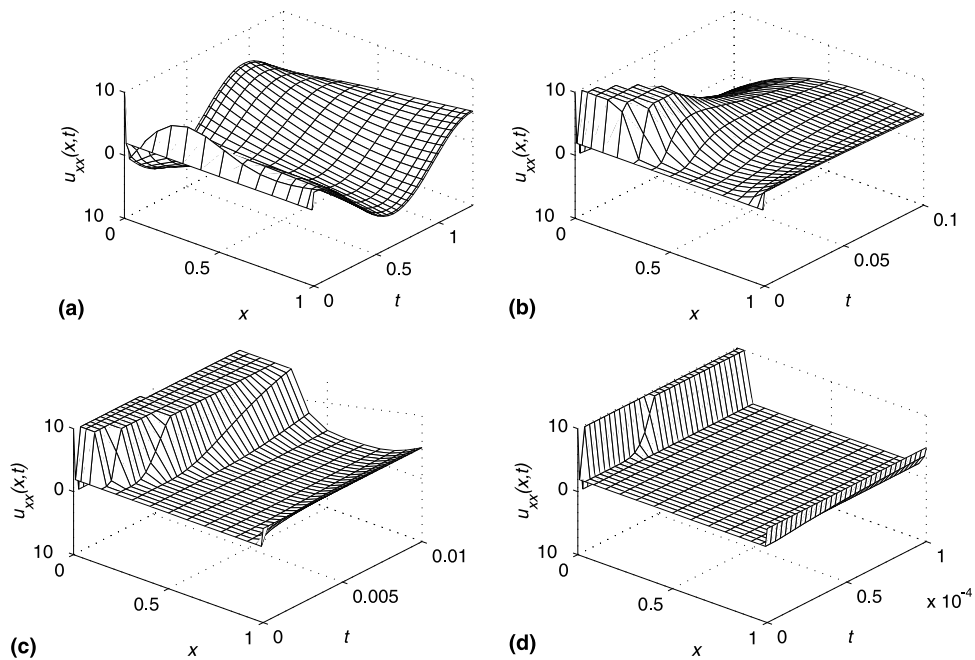


Fig. 4. Analytic values for  $u_{xx}$  ( $= u_t$ ) for Example 2 over four different intervals in  $t$  (a)  $[0, \frac{4}{\pi}]$ , (b)  $[0, 10^{-1}]$ , (c)  $[0, 10^{-2}]$ , (d)  $[0, 10^{-4}]$ . The surfaces are truncated in height at the level  $u_{xx} = 10$ .

from a stability condition of the form  $\Delta t \leq \text{const}/N^4$ , it is also quite ineffective in increasing the accuracy. Chebyshev methods are only spectrally accurate when solutions are smooth and, in the corners, this is not the case. If we measure errors at grid points only (meaning that for larger  $N$ , we get grid points moving closer to the singularity), the improvement in max norm error by increasing  $N$  is almost nonexistent. In Example 2, increasing  $N$  from 11 up to 51 brings the error down only from 0.05 to 0.03. Refining a Chebyshev grid to capture a singularity more accurately is a conceptually unsound approach, since the problem is one of multiple spatial scales. The initial condition is given on a large space scale, and the corner singularities first appear on extremely small scales. Separating the two issues from each other, as we will be doing, allows each one to be handled in a way that is optimized for its particular scale and character.

#### 4. Correction procedure

For simplicity of notation, we describe the correction procedure not in full generality, but instead in terms of Example 2 from Section 3, i.e., as defined by (1), (6), and (9). Table 1 summarizes the quantities that should be zero at the two corners, and lists the values which we instead observe from the given IC and BC data. The first step in the correction procedure is to reproduce the corner discrepancies using the basis functions  $u_k(x, t)$  introduced in Section 2. Therefore, we form the function

$$s(x, t) = \left\{ \frac{1}{0!} u_0(x, t) - \frac{2}{1!} u_1(x, t) - \frac{\pi^4}{4 \cdot 2!} u_2(x, t) + \frac{\pi^8}{16 \cdot 4!} u_4(x, t) \right\} \\ + \left\{ \frac{\pi^2/2 - 2}{1!} u_1(1-x, t) - \frac{\pi^6}{8 \cdot 3!} u_3(1-x, t) \right\}. \quad (11)$$

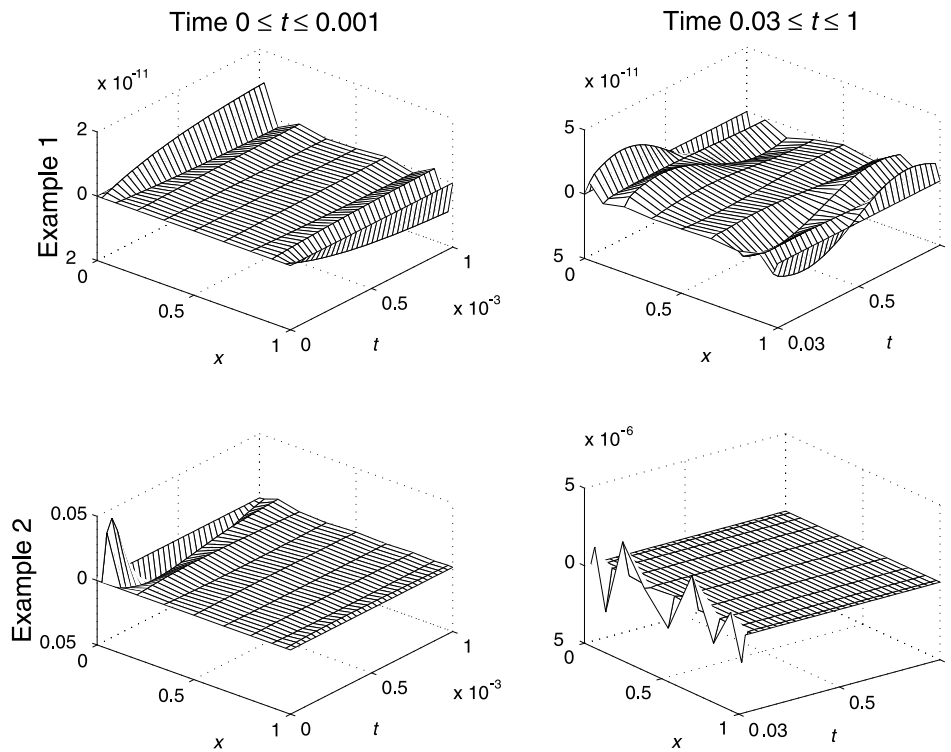


Fig. 5. Errors in CPS solution (with  $N = 11$  points in space) for the two examples displayed over the time intervals  $0 \leq t \leq 0.001$  (left column) and  $0.03 \leq t \leq 1$  (right column).

Table 1  
Summary of leading order corner discrepancies for Example 2, Section 3

Quantities that should be zero according to the PDE	Values of the different quantities, as obtained by BC and IC information	
	At left corner ( $x = 0, t = 0$ )	At right corner ( $x = 1, t = 0$ )
$u - u$	1	0
$u_t - u_{xx}$	-2	$\pi^2/2 - 2$
$u_{tt} - u_{xxxx}$	$-\pi^4/4$	0
$u_{ttt} - u_{xxxxx}$	0	$-\pi^6/8$
$u_{tttt} - u_{xxxxxx}$	$\pi^8/16$	0
...	...	...

Recalling, for instance at  $x = 0$ , that  $u_k(0, t) = t^k$ , i.e.,  $1/(k!)/\partial^k u_k(0, t)/\partial t^k = 1$ , the coefficients of  $s(x, t)$  are simply the magnitude of the corner discrepancies divided by  $k!$ . Since  $u_k(x, t)$  is bounded in size by  $t^k$ , using four basis functions will prove to be more than enough to achieve computer accuracy for small  $t$ . The function  $s(x, t)$

- is analytically available (it will be shown in Section 5 that this is not necessary to implement the correction procedure),
- satisfies the PDE (1),
- satisfies the IC  $s(x, 0) = 0$ ,
- has, to the orders included, the same corner singularities as the desired solution.

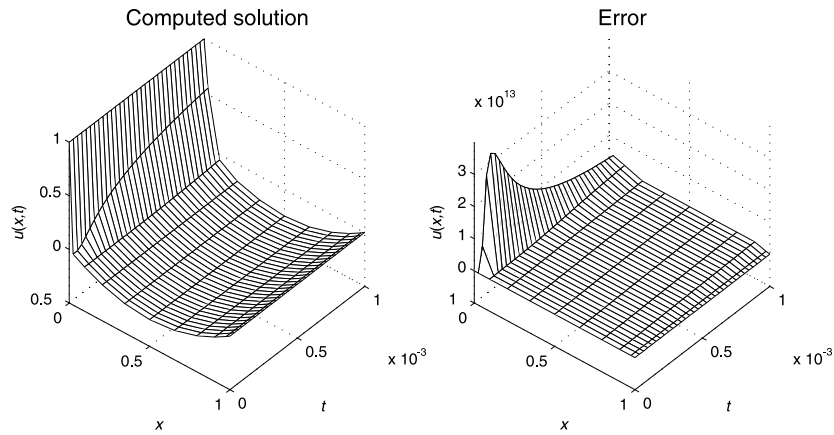


Fig. 6. Computed solution and error up to time  $t = 0.001$  for Example 2, with the correction procedure implemented.

To solve our PDE (1) with the BC (6) and the IC (9), we next consider

$$v(x, t) = u(x, t) - s(x, t). \quad (12)$$

This function  $v(x, t)$  satisfies

- the PDE  $v_t = v_{xx}$ ,
- the same IC as  $u(x, t)$  (since  $s(x, 0) = 0$ ),
- the same BC as  $u(x, t)$ , however with the boundary values for  $s(x, t)$  (as obtained from (11)) subtracted.

Our procedure for correcting the corner singularities consists of numerically solving the corresponding IBVP for  $v(x, t)$  and then adding back  $s(x, t)$  to obtain the solution for  $u(x, t)$ . The whole point with first subtracting the function  $s(x, t)$  and then adding it back is, of course, that the function  $v(x, t) = u(x, t) - s(x, t)$  (on which we do the actual numerics) has been made free of the corner singularities up to a high order. Fig. 6 (for CPS, again with  $N = 11$ ) has been obtained with this correction implemented. The left subplot shows the computed solution over the time  $[0, 0.001]$  and the right subplot displays the error (which should be compared against the equivalent error without correction, as showed at bottom left in Fig. 5. With the correction procedure, the error has been reduced from 0.05 to  $O(10^{-13})$ . After the initial transients have died down, the correction procedure is unnecessary and the regular CPS method can be applied directly to the PDE solution  $u(x, t)$ .

## 5. Generalization to variable coefficients

The concept of singularity subtraction is effective in all cases. But for variable coefficients, it is only in rare cases that we have very simple closed-form expressions like (5) to work with.

### 5.1. PDEs of the form $u_t = a(t)u_{xx}$

The change of variable  $\tau = \int_0^t a(t) dt$  transforms this PDE into  $u_\tau = u_{xx}$ . Therefore, substituting  $\int_0^t a(t) dt$  in place of  $t$  wherever this independent variable appears in the right hand sides of (5) will give us the appropriate set of corner functions for this particular variable coefficient case. The resulting functions will all satisfy the PDE and the IC  $u_k(x, t) = 0$ . The boundary condition at  $x = 0$  has however become slightly modified, to  $u_k(0, t) = (\int_0^t a(t) dt)^k$ . After a brief Taylor expansion in  $t$ , this form is seen to be just as suitable to work with as  $u_k(0, t) = t^k$  was in the constant coefficient case.

5.2. PDEs of more general form

For general 1-D convection–diffusion equations, the corner singularity functions  $u_k(x, t)$  can be computed rapidly and conveniently following a change of variables. For simplicity, we will explain this first in the case of the constant coefficient heat equation (1). Fig. 7 shows some contour lines for the function  $u_0(x, t)$ . For increasing values of  $t$ , this function gets uniformly stretched out in the  $x$ -direction proportionally to  $\sqrt{t}$  (as can also be seen directly from its closed form (4)). This suggests a change of variable

$$\xi = \frac{x}{\sqrt{t}}.$$

Then,  $u_x = \frac{1}{\sqrt{t}}u_\xi$  and  $u_{xx} = \frac{1}{t}u_{\xi\xi}$ , so the heat equation (1) now becomes  $u_t = \frac{1}{t}u_{\xi\xi}$ . To get rid of the  $\frac{1}{t}$ -factor, we let

$$\tau = \log t.$$

Then  $u_t = u_\xi \xi_t + u_\tau \tau_t = -\frac{1}{2} \frac{x}{t\sqrt{t}}u_\xi + \frac{1}{t}u_\tau$  and the equation becomes

$$u_\tau = u_{\xi\xi} + \frac{1}{2}\xi u_\xi. \tag{13}$$

With the boundary conditions  $u(0, \tau) = 1$ ,  $u(\infty, \tau) = 0$ , the equilibrium solution becomes  $u(\xi) = \text{Erfc}(\xi/2)$ , confirming that (13) indeed generates the corner singularity function  $u_0(x, t)$ . With the left boundary condition  $u(0, \tau) = e^{k\tau}$  (since  $t^k = e^{k\tau}$ ), we similarly obtain  $u_k(x, t)$ ,  $k = 0, 1, \dots$ . Eq. (13) is very well suited for numerical implementation:

- it has no singularities or mixing of scales due to the  $\tau$  domain starting at  $\tau = -\infty$
- the solutions decay to zero extremely rapidly for increasing  $\xi$ , so a small  $\xi$ -interval is sufficient even for very high accuracies,
- the small number of grid points that is needed for a Chebyshev discretization in space (maybe 10 or so) means that we can easily afford implicit (unconditionally stable) time stepping, if we so wish.

The fact that we do not have any obvious initial condition for (13) matters little; we simply start at some negative  $\tau$ -position (exactly where would depend on the accuracy we want) and the character of the

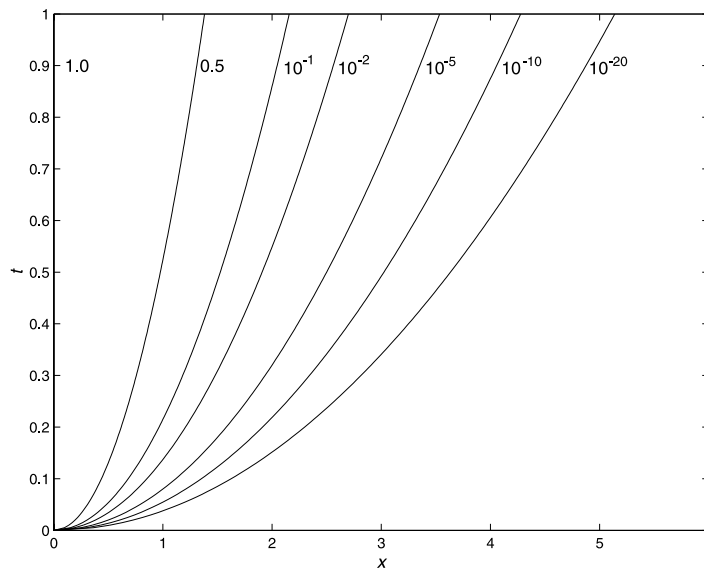


Fig. 7. Some contour lines for  $u_0(x, t)$ .

equation is such that it quickly wipes out the effects of any bad initial conditions we might have chosen. Suppose next that our original heat equation has variable coefficients, for example  $u_t = a(x, t) u_{xx}$ . Instead of (13), we then obtain

$$u_\tau = a(\xi e^{\tau/2}, e^\tau) u_{\xi\xi} + \frac{1}{2}\xi u_\xi.$$

Although we no longer have any equilibrium solution and are unlikely to find any analytical solution, nothing of numerical significance has changed—this is again a PDE very well suited for numerics. Other variations (which also can include a convection term) can be handled similarly. For example,  $u_t = (a(x, t) u_x)_x$  leads to  $u_\tau = a u_{\xi\xi} + (\frac{\xi}{2} + a_\xi) u_\xi$ , and  $u_t = a(x, t) u_{xx} + b(x, t) u_x + c(x, t) u$  leads to  $u_\tau = a u_{\xi\xi} + (\frac{\xi}{2} + b e^{\tau/2}) u_\xi + c e^\tau u$ , etc. Since we are only interested in solving these PDEs for  $\tau$ -ranges well below  $\tau = 0$  (corresponding to very small positive  $t$ -values), the exponentials  $e^{\tau/2}$  and  $e^\tau$  are very close to zero).

### 5.3. Numerical example

As an example of implementing the above technique, consider the following variable coefficient case

$$\begin{aligned} u_t &= (\tanh(3x + 0.5)u_x)_x, \\ u(0, t) &= \sin\left(\frac{\pi^2}{2}t\right), \quad u(1, t) = 0, \\ u(x, 0) &= \sin(\pi x). \end{aligned} \tag{14}$$

The PDE models diffusion through a media that has a sharp gradient in its permeability, represented by the tanh profile. The subtlety in this problem is that, although the IC is consistent with the BCs to leading order (both are zero at  $x = 0$  and  $x = 1$ ), they are inconsistent with the PDE and its higher derivatives. Letting  $L = (\partial/\partial x)(\tanh(3x + 0.5)(\partial/\partial x))$ , the leading order compatibility conditions require that the following quantities are zero at the two corners

- (i)  $u - u = 0$ ,
- (ii)  $u_t - Lu = 0$ ,
- (iii)  $u_{tt} - L(Lu) = 0$ ,
- (iv)  $u_{ttt} - L(L(Lu)) = 0$ .
- ... ..

Tables 2 and 3 summarize how these conditions are violated due to the present IC and BC. The correction functions are obtained via the CPS method by applying the IC  $u(\xi, \ln(10^{-5})) = 0$  and the BC  $u(0, \tau) = e^{k\tau}$  (where  $k$  is the order of the correction function) to (14) in  $\xi, \tau$  coordinates. For the left corner, this becomes

Table 2  
Leading order corner discrepancies at left corner for the variable coefficient case, Section 5.3, ( $x = 0, t = 0$ )

Incompatibilities between the IC and BCs as obtained from the PDE and its differentiated forms	
(i)	0
(ii)	$\pi^2/2 - 3\pi \operatorname{sech}^2(0.5)$
(iii)	$6\pi(27 + \pi^2 + (\pi^2 - 9) \cosh(1)) \operatorname{sech}^4(0.5) \tanh(0.5)$
(iv)	$-\pi^6/8 + \frac{27\pi}{32} \operatorname{sech}^8(0.5) [34560 + 544\pi^2 + 2\pi^4 + (-39600 + 52\pi^2 + \pi^4) \cosh(1) - 2(-3168 + 224\pi^2 + \pi^4) \cosh(2) + (-144 + 44\pi^2 - \pi^4) \cosh(3)]$
...	...

Table 3  
Leading order corner discrepancies at right corner for the variable coefficient case, Section 5.3, ( $x = 1, t = 0$ )

Incompatibilities between the IC and BCs as obtained from the PDE and its differentiated forms	
(i)	0
(ii)	$3\pi \operatorname{sech}^2(3.5)$
(iii)	$-6\pi(27 + \pi^2 + (\pi^2 - 9) \cosh(7)) \operatorname{sech}^4(3.5) \tanh(3.5)$
(iv)	$-\frac{27\pi}{32} \operatorname{sech}^8(3.5) [34560 + 544\pi^2 + 2\pi^4 + (-39600 + 52\pi^2 + \pi^4) \cosh(7) - 2(-3168 + 224\pi^2 + \pi^4) \cosh(14) + (-144 + 44\pi^2 - \pi^4) \cosh(21)]$
...	...

$$u_\tau = \tanh(3\xi e^{\tau/2} + 0.5) u_{\xi\xi} + \left(\frac{1}{2}\xi + 3 \operatorname{sech}^2(3\xi e^{\tau/2} + 0.5) e^{\tau/2}\right) u_\xi.$$

As noted above, and seen in Fig. 8, the correction functions decay rapidly not only in  $x$ , but also in  $\xi$ . We therefore need only a small  $\xi$  interval. Since the solution is free of singularities in the  $\xi, \tau$ -plane, a small number of grid points, here 11, suffices for the computation. We can also see that the influence of an inaccurate IC in the  $\xi, \tau$ -plane computation (here for convenience chosen as identically zero) becomes quickly self-corrected. Chebyshev interpolation is particularly convenient for transferring the solution over to grid positions in the  $x$ -direction (In time, no interpolation at all is needed if our  $\tau$ -steps are suitably chosen). The dependence of these correction functions,  $u_k(x, t)$ , solely on the PDE implies the following:

- The BCs and IC of the problem can be changed without having to re-compute the correction functions.
- As a result, the correction functions only need to be computed once and stored for a given PDE.

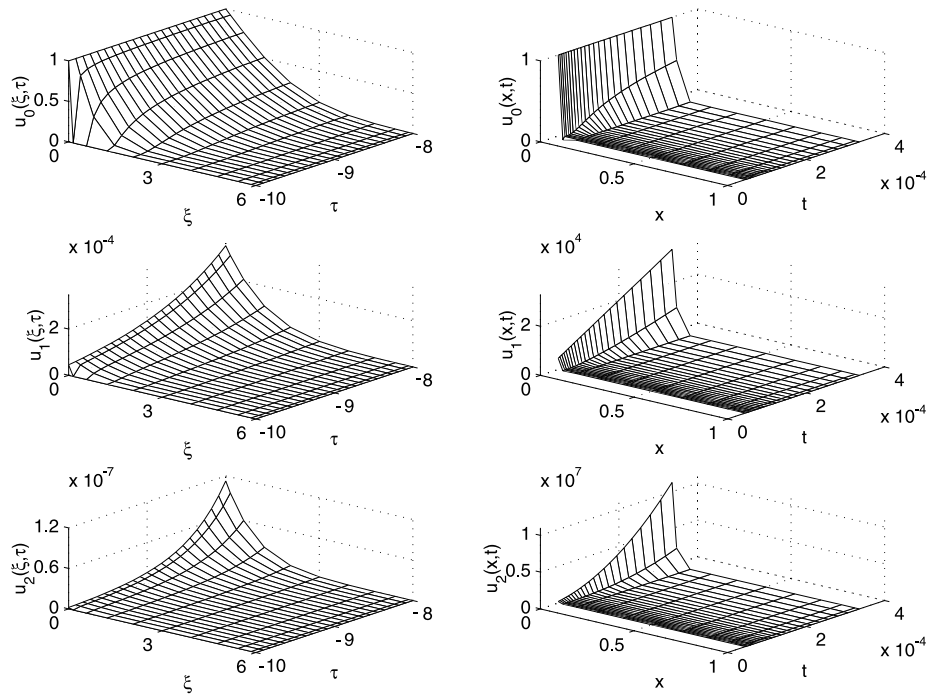


Fig. 8. Left corner correction functions  $u_0, u_1, u_2$  to (14), shown as computed in the  $\xi, \tau$ -plane (left column) and when interpolated to the  $x, t$ -plane (right column).

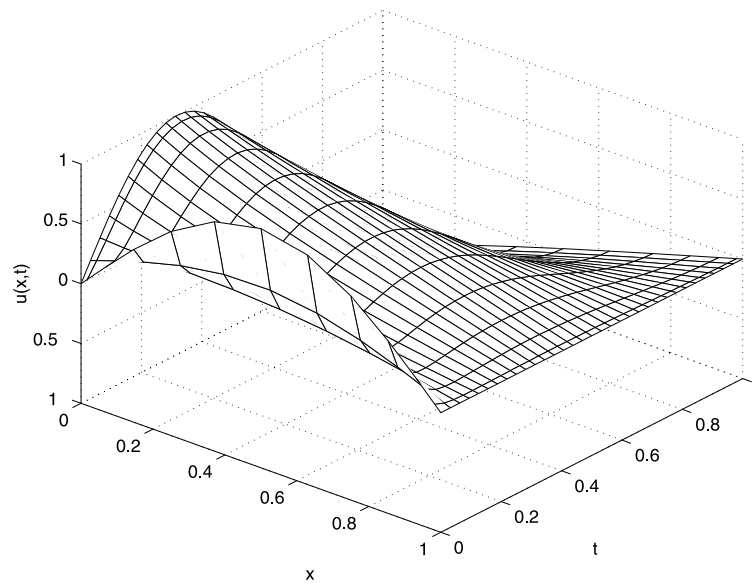


Fig. 9. The numerical solution  $u(x,t)$  to (14) for  $0 \leq t \leq 1$ .

- Changing the PDE being solved only requires a change in one line of code for calculating the new correction functions.

Since the correction functions reconstruct the corner singularities, they are only implemented during the initial transient period of the solution. For longer time we can directly integrate (14). The solution is shown in Fig. 9.

## 6. Concluding remarks

When solving initial-boundary value problems, singularities almost always occur in the corners where IC and BC meet. For dissipative PDEs, these singularities are confined to the corners of the time–space domain. In general, if we are interested in numerical solutions only at large times, they can safely be ignored. The dissipative process of the PDE is ‘self-correcting’ in the sense that accurate long-term solutions do not depend on catching initial details accurately. However, for applications in which these initial gradients are of interest, it is far more efficient to utilize a method that is designed to correct for them rather than increasing the overall computational resolution until short-term errors also become sufficiently small (or than to use a boundary-layer approach which would be forced to simultaneously deal accurately with features on very different length scales). In our examples,  $N = 11$  grid points in space was sufficient to obtain better than  $10^{-10}$  level accuracy. The spectral convergence implies that the accuracy could have been further increased with only very small changes in  $N$ . For instance in Example 2 in Section 3, we find

$N$	9	10	11	12	13
Max norm error	$1 \times 10^{-8}$	$5 \times 10^{-10}$	$4 \times 10^{-11}$	$1 \times 10^{-12}$	$4 \times 10^{-14}$

In an application, one may need to obtain the solution at a different point set than just on a coarse Chebyshev grid. The present approach separates the smooth and the singular parts of the solution in a way

such that both are smooth on their respective grids. This is in contrast to the situation if the problem had been solved using Chebyshev mesh refinement or some boundary-layer method. In this study, we have illustrated the phenomenon of initial time–space corner singularities in the case of the 1-D convection–diffusion equation. We then devised and demonstrated the effectiveness of a correction procedure that is based on separating the small corner scale of the problem from the large scale solution. The key feature of this approach is to identify the corner singularities and to treat them separately from the solution to the rest of the PDE. The major advantages of this include:

- In cases such as constant coefficients or with a variable coefficient that only depends on time, the corner singularities can be found analytically at essentially no additional computational cost. Full precision results will be obtained just as effectively at very short times as at long times.
- We can interpolate our solutions over to other grids (than the coarse Chebyshev one used in the actual calculation) with little or no loss of accuracy even in the immediate vicinity of the singularities.
- If our PDE has variable coefficients, we can cheaply and accurately compute the relevant corner singularity functions. A change of variables leads to a numerically easy-to-solve PDE describing them.
- The corner singularity functions depend on the PDE's variable coefficients, but not on initial and boundary conditions. Once these singularity functions are computed and stored away (only about 4 or so in total are needed), they can be re-used indefinitely whenever initial and boundary conditions change.

## References

- [1] J.P. Boyd, N. Flyer, Compatibility conditions for time-dependent partial differential equations and the rate of convergence of Chebyshev and Fourier spectral methods, *Comput. Meth. Appl. Mech. Eng.* July (1999) 281–309.
- [2] B. Chambers, T.Y.T. Lee, W. Blood, Steady state and transient thermal analysis of chip scale packages, *J. Electron. Manf.* 9 (2) (1999) 131–139.
- [3] N. Flyer, P. Swartztrauber, Convergence of spectral and finite difference methods for initial-boundary value problems, *SIAM J. Sci. Comput.* 23 (5) (2002) 1731–1751.
- [4] B. Fornberg, *A Practical Guide to Pseudospectral Methods*, Cambridge University Press, Cambridge, 1996.
- [5] S.H. Gilbert, L.E. Ford, Heat changes during transient tension responses to small releases in active frog muscle, *Biophys. J.* 54 (1988) 611–617.
- [6] W.M. Schikorr, Assessments of the kinetic and dynamic transient behavior of sub-critical systems (ADS) in comparison to critical reactor systems, *Nucl. Eng. Des.* 210 (1–3) (2001) 95–123.
- [7] I. Kocabas, M.R. Islam, Concentration and temperature transients in heterogeneous porous media Part I: Linear transport, *J. Petrol. Sci. Eng.* 26 (1–4) (2000) 211–220.